The effect of an asymmetric core on convection in Enceladus' ice shell: Implications for south polar tectonics and heat flux

Adam P. Showman,[1] Lijie Han,[2] and William B. Hubbard[1]

Received 28 June 2013; revised 4 October 2013; accepted 6 October 2013.

[1] Enceladus exhibits a strong tectonic contrast between its south polar terrain (SPT), which is young and geologically active, and its northern hemisphere, which is relatively ancient and stable. Previous global three-dimensional (3-D) spherical models of convection exhibit patterns that are symmetrical around the equator and fail to explain the formation of a hemispheric dichotomy. Here we present global 3-D spherical models of convection in Enceladus' ice shell to show that convection in Enceladus' ice shell with plasticity and irregular core geometry can self-consistently generate a hemispheric dichotomy in tectonics and heat flux. With a spherical core, convection produces global overturning, which cannot explain the regional confinement of Enceladus' current tectonic activity to the SPT. Models with appropriate nonspherical core geometry and plasticity tend to produce overturning confined to the SPT or regional overturning in different regions at different times, which can explain the tectonic dichotomy and local age differences on Enceladus. Our models predict heat flows up to 5–10 gigawattts (GW) during active episodes, consistent with Cassini observations. **Citation:** Showman, A. P., L. Han, and W. B. Hubbard (2013), The effect of an asymmetric core on convection in Enceladus' ice shell: Implications for south polar tectonics and heat flux, *Geophys. Res. Lett.*, *40*, doi:10.1002/2013GL057149.

1. Introduction

[2] In contrast with the cratered northern terrains, Enceladus' southern hemisphere is highly active. The south polar terrains (SPT) are heavily tectonised and exhibit surface ages of 10–100 Myr or less [*Porco et al.*, 2006]. The "tiger stripes," four ∼130 km long fractures that dominate the SPT, exhibit a total heat flow of 15.8 ± 3.1 GW [*Howett et al.*, 2011]. Jets of salty ice particles [*Postberg et al.*, 2011] and various gases [*Waite et al.*, 2009] emanate from the tiger stripes, indicating intense current activity. The heat presumably results from tidal dissipation caused by the orbital resonance between Enceladus and Dione [*Meyer and Wisdom*, 2007, 2008], although the details remain poorly understood. Many authors have suggested that convection in the ice shell transports the internally dissipated heat to the surface and promotes the intense tectonism observed in the SPT [*Grott et al.*, 2007; *Barr and McKinnon*, 2007; *Mitri and Showman*, 2008; *Roberts and Nimmo*, 2008; *Tobie et al.*, 2008; *Běhounková et al.*, 2010; *O'Neill and Nimmo*, 2010]; once weakened, shear heating along fractures such as the tiger stripes can also contribute [*Nimmo et al.*, 2007].

[3] However, previous models have failed to explain the confinement of the high heat flux and recent tectonism to the southern hemisphere. Three-dimensional models of thermal convection in Enceladus' ice shell with no imposed asymmetries exhibit multiple ascending and descending plumes and lack any contrast between the two hemispheres [*Roberts and Nimmo*, 2008; *Běhounková et al.*, 2010; *Han et al.*, 2012]. Several authors have explored the conditions under which imposed asymmetries between the hemispheres, such as an imposed subsurface ocean or weak zone at the south pole, can explain the enhanced activity within the SPT [*Tobie et al.*, 2008; *Běhounková et al.*, 2012; *Han et al.*, 2012]. Although these models offer important insights, they suffer from the chicken-and-egg difficulty that some manifestation of activity (weak SPT or subsurface ocean) must be imposed to explain other aspects of activity (high heat flux).

[4] Here we present global, 3-D spherical models of thermal convection showing that the existence of appropriate topography on Enceladus' silicate core can modulate the convection and naturally lead to enhanced activity at the south pole. The asymmetry in tectonics and heat flux emerges spontaneously from the asymmetry in the core-ice-shell boundary and does not require any ad hoc thermal anomalies, oceans, or pre-imposed weakening in the ice shell.

2. Model

[5] We solve the Boussinesq convection equations in a global, 3-D spherical ice shell with inner and outer radii of 150 and 250 km appropriate to a differentiated Enceladus. To investigate the effects of brittle deformation, we include plastic rheology. Plastic deformation occurs only when deviatoric stresses reach a specific yield stress σ_Y [*Moresi and Solomatov*, 1998; *Tackley*, 2000]. The plasticity is incorporated by means of an "effective viscosity" [*Showman and Han*, 2005], $\eta_{\rm eff}$, defined as

$$\eta_{\rm eff} = \min\left[\eta(T), \frac{\sigma_Y(z)}{2\dot{\epsilon}}\right] \quad (1)$$

where $\eta(T)$ is the temperature-dependent creep viscosity implemented as in *Han et al.* [2012], $\dot{\epsilon}$ is the second invariant of the strain rate tensor, and σ_Y is the yield stress, which is constant in the bottom 90% of the domain and decreases near the surface as in *Showman and Han* [2005]. Some models include constant tidal heating at amplitudes appropriate to the current eccentricity, but this does not affect our qualitative conclusions.

[1]Department of Planetary Sciences, Lunar and Planetary Laboratory, University of Arizona, Tucson, Arizona, USA.
[2]Planetary Science Institute, Tucson, Arizona, USA.

Corresponding author: A. P. Showman, Department of Planetary Sciences, Lunar and Planetary Laboratory, University of Arizona, Tucson, AZ 85721, USA. (showman@lpl.arizona.edu)

0094-8276/13/10.1002/2013GL057149

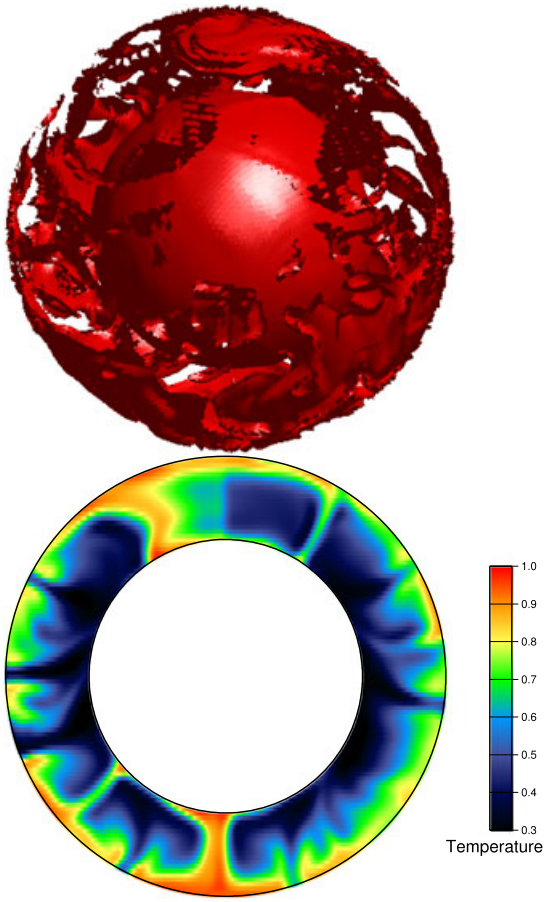

Figure 1. Temperature structure from a full 3-D spherical model showing thermal convection in Enceladus' ice shell during a lithospheric overturn event. The simulation adopts a Rayleigh number of 5×10^7, a viscosity contrast $\Delta\eta = 10^5$, and a yield stress of 0.1 bar. (top) A 3-D temperature structure with a temperature isosurface of 230 K is displayed. (bottom) Temperature distribution along a radial cross section is also displayed. In the simulation, a stagnant lid builds, then undergoes a global overturn (shown), after which the stagnant lid regrows, and the cycle repeats episodically. In the absence of core topography, the overturns are usually global as shown here.

[6] We solve the equations using the finite-element code CitcomS [*Zhong et al.*, 2000] with a grid resolution of $48 \times 48 \times 48$ in each of the model's 12 subdomains (corresponding to a resolution of 1.5° in longitude and latitude). Isothermal boundary conditions are imposed at the top and bottom of the ice shell. Velocity boundary conditions are free-slip on the top and no-slip or partially no-slip at the bottom. The initial condition is a conductive thermal profile with a degree-1, order-0 perturbation, of amplitude 15 K, placed at the bottom to initiate convection.

3. Results

[7] First, we consider models with a spherical core geometry. When the yield stress is large ($\sigma_Y \geq 0.2$ bar), the convection occurs under a thick stagnant lid, if at all; the heat flux is small (~5–10 mW m^{-2}) and there is no hemispheric dichotomy in convection. At sufficiently small yield stresses (0.1–0.2 bar), however, the plasticity allows episodic overturning of the lid, consistent with the results of 2-D studies [*Moresi and Solomatov*, 1998; *Showman and Han*, 2005]. The stagnant-lid thickness builds until stresses reach the yield stress, whereupon plastic deformation causes the lid to overturn and allows warm, mobile ice to reach the near-surface. Figure 1 illustrates an example. Our 3-D models show that episodic overturning events, even if locally initiated, tend to rapidly expand into full global overturns. On Enceladus, this would lead to similar tectonics and ages across the entire surface, inconsistent with observations.

[8] The global nature of episodic overturning events in our 3-D models with spherical cores contrasts with the suggestion of *O'Neill and Nimmo* [2010] from two-dimensional (2-D), Cartesian regional models that such overturning events might be regionally confined. Generally, previous 2-D models show that, when the viscosity contrast is realistically large, episodic overturning occurs over only a narrow range of yield stresses [*Moresi and Solomatov*, 1998, Figure 4]. Previous 2-D models of icy-satellite convection

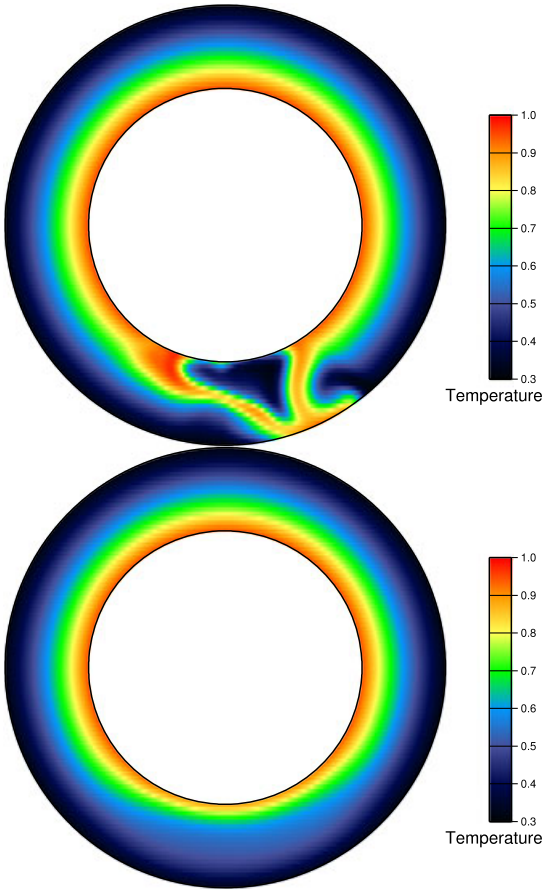

Figure 2. Temperature distribution along a radial cross section from a full 3-D spherical model, including core topography of degree 1, order 0, and an amplitude of 14 km, showing the confinement of an overturning event to the south polar terrain. The simulation adopts a reference Rayleigh number of 5×10^7, a viscosity contrast $\Delta\eta = 10^5$, and a yield stress of 0.1 bar. The overturns occur periodically, as in Figure 1, but here they occur only southward of ~60°S latitude. (top) Overturning happens in the SPT. (bottom) Stagnant-lid stage in the SPT.

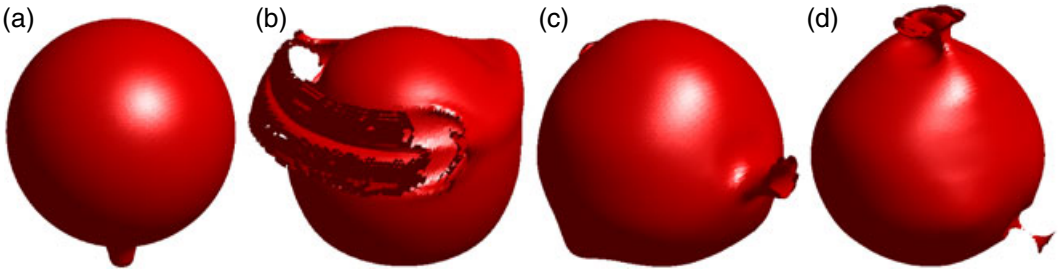

Figure 3. Temperature structure from a full 3-D spherical model, with a core topography of degree 3, order 0, and an amplitude of 10 km, showing localization of overturning events not only to the SPT but to other local regions as well. The simulation adopts a reference Rayleigh number of 7×10^7, a viscosity contrast $\Delta\eta = 10^5$, and a yield stress of 0.1 bar. This particular model includes a free-slip bottom boundary condition southward of 60°S to represent a subsurface ocean underlying the SPT. Simulations with a variety of bottom boundary-condition types show that topography has the strongest influence. The figure displays the temperature distribution on an isosurface of 230 K. The overturns occur regionally in different places at different times, including (a) the SPT, (b) the mid-northern latitudes, (c) the equator, and (d) the north pole and southern hemisphere.

with plasticity by *Showman and Han* [2005] also suggest that such overturnings tend to occur over the entire domain rather than regionally. As *O'Neill and Nimmo* [2010] emphasize, realistic spherical geometry may influence the behavior of the overturns, and understanding the confinement of Enceladus' activity to the SPT therefore requires 3-D spherical models. However, our 3-D models with spherical cores failed to produce regionally confined overturns.

[9] As pointed out by *McKinnon* [2013], asteroids similar in size to Enceladus (e.g., Pallas, Hygiea, and Vesta) exhibit irregular shapes, and under conditions relevant to Enceladus, a silicate core can maintain topography indefinitely. Moreover, Cassini observations show that Enceladus deviates from the shape of an equilibrium oblate spheroid, perhaps due in part to a nonspherical core [*McKinnon*, 2013]. Motivated by these issues, we consider the effect of core topography on convection in the ice shell. Suppose the core topography measured relative to the bottom of the simulation domain is $h(\theta, \phi)$, where θ is colatitude and ϕ is longitude. To represent the effect of core topography, we introduce a viscosity contrast of 10^{10} for all regions at and below the height $h(\theta, \phi)$, thereby limiting ice flow to regions outside of that surface. Simple estimates show that, in hydrostatic equilibrium, core topography leads to surface topography less than 10–30% in amplitude of the core topography (see Appendix). For simplicity, we therefore neglect the surface topography variation in our models.

[10] We find that appropriate global wave number 1 topography, with the ice shell slightly thicker at the south pole than elsewhere, can allow convection to occur preferentially at the south pole. Figure 2 illustrates an example with core topography of 14 km—consistent with topographic amplitudes suggested by *McKinnon* [2013]—and a yield stress $\sigma_Y = 0.1$ bar. The convection occurs and, importantly, is confined to regions near the south pole. The stagnant lid grows, becomes locally unstable, and overturns—*but only regionally near the south pole*. After the regional overturn, the stagnant lid regrows in the affected area and the cycle repeats. No convection occurs in Enceladus' northern hemisphere, consistent with the relatively ancient ages of most terrains there. This model can naturally explain the confinement of Enceladus' activity to the SPT.

[11] Our model can explain the hemispheric heat flux dichotomy on Enceladus. Because convection is confined to the SPT, the heat flux in the northern hemisphere is low (∼5–10 mW m^{-2}), while the heat flux in the SPT can experience episodic spikes. Our model can also explain the apparent contradiction between the current massive heat flux and the limited total power budget available to Enceladus. In our models, the heat flow rate at the SPT during the overturn reaches 5–10 GW, consistent with the observed heat flow. Nevertheless, because the overturn events typically occur during only ∼5% of the total history, the *time-mean* heat flux is relatively low. Thus, our models help to resolve the conundrum that, for realistic orbital histories, the available tidal heating on Enceladus is too small to maintain the observed heat flux in steady state [*Meyer and Wisdom*, 2007].

[12] Models with appropriate core topography can produce overturning events that are localized but occur in different places at different times. Figure 3 illustrates an example with core topography of degree 3, order 0, and amplitude of 10 km. Convection initiates at the SPT, then switches to the

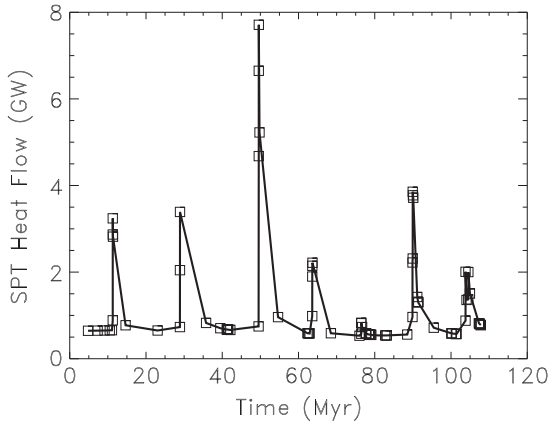

Figure 4. SPT heat flow over time in the simulation from Figure 3. Heat flow is integrated over the region south of 60°S latitude. The episodic nature of the heat flow helps to reconcile the current high heat flow with orbital and evolutionary constraints on Enceladus' time-integrated power budget.

northern hemisphere, and switches back to the SPT again later. The overturns, while occurring in various locations, remain regionally confined—unlike our models without core topography. Figure 4 demonstrates the episodic nature of the heat flow in these models. These results can explain the fact that—despite current confinement of activity to the SPT—tectonism occurred in the ancient past in other regions [*Kargel and Pozio*, 1996; *Crow-Willard and Pappalardo*, 2011], accompanied by enhanced heat fluxes [*Bland et al.*, 2007, 2012]. Moreover, these results are consistent with Cassini gravity observations showing that J_3 is negative on Enceladus [*Ducci et al.*, 2012], as would be expected to occur if core topography caused a negative gravity anomaly near the south pole.

4. Conclusions

[13] Previous 3-D models have proved unable to explain the localization of activity on Enceladus to south polar regions. We argue that this conundrum resolves if the silicate core is slightly aspherical, and we presented global, 3-D convection models including plastic deformation to demonstrate the mechanism. For sufficiently low yield stresses, the ice shell can exhibit episodic overturns, which would cause intense tectonism and heat flux in the affected area. Although the required yield stresses are lower than those typically measured in the laboratory, they are compatible with previous yield stress estimates for icy satellites [*Hoppa et al.*, 1999; *Olgin et al.*, 2011]. Our models show that, with appropriate core topography, these overturns can be localized to the SPT, or occur episodically in different places in different times. In contrast, overturns in models without core topography are generally global, inconsistent with observations. Recent gravity data, including a negative J_3, are consistent with this scenario. Better characterization of Enceladus' gravity field by *Cassini* or future orbiters can help to further test our ideas.

Appendix A: Two-Layer Enceladus Model

[14] Consider a two-layer model of Enceladus with a silicate core of constant density ρ_c overlain by an ice mantle of constant density ρ_m. The shape of either core-mantle boundary (CMB) or the satellite surface can be described by

$$r_i(\theta,\phi) = a_i + \sum_{l=1}^{\infty}\sum_{m=-l}^{l} \delta r_{i,lm} Y_{lm}(\theta,\phi) \qquad \text{(A1)}$$

where the index i refers either to the core (subscript c) or satellite surface (subscript s). Here a_i is a constant mean radius (of the core or satellite), Y_{lm} are spherical harmonics of degree l and order m, θ is colatitude, ϕ is longitude, and $\delta r_{i,lm}$ are the prescribed topographic coefficients, for a given spherical harmonic, of either the CMB or satellite surface.

[15] A silicate core is sufficiently rigid that it should maintain its shape over Solar System history [e.g., *McKinnon*, 2013], but, given the tidal heating in Enceladus' ice shell, we would expect the satellite surface to be close to an equipotential (ignoring the dynamic topography associated with mantle convection). The gravitational potential can be represented as the superposition of the potential due to a homogeneous body of constant density ρ_m and shape $r_s(\theta,\phi)$ and that of another homogeneous body of constant density $\rho_c - \rho_m$ and shape $r_c(\theta,\phi)$. Equating this potential to the equipotential of the surface, GM/r_s, which we assume to be constant, yields the following expression for the shape of the satellite surface:

$$\frac{\delta r_{s,lm}}{a_s} = \frac{3}{2l+1}\frac{4\pi(\rho_c-\rho_m)a_c^3}{3M}\left(\frac{a_c}{a_s}\right)^l \frac{\delta r_{c,lm}}{a_c} \times \left[1 - \frac{3}{2l+1}\frac{4\pi\rho_m a_s^3}{3M}\right]^{-1} \qquad \text{(A2)}$$

where G is the gravitational constant and M is the mass of Enceladus. For Enceladus parameters (a_c = 150 km, a_s = 250 km, ρ_c = 3000 kg m^{-3}, ρ_m = 1000 kg m^{-3}, M = 1.08 × 10^{20} kg), this expression yields $\delta r_{s,lm}/\delta r_{c,lm}$ of 0.4, 0.09, 0.03, and 0.014 for l = 1, 2, 3, and 4, respectively, with even smaller values for $l \geq 5$. Thus, for all harmonics except l = 1, the surface topography in gravitational equilibrium with specified core topography is small. In a 3-D mantle convection model, it is thus a reasonable zeroth-order approximation to include core topography while ignoring the deformation associated with the satellite surface.

[16] **Acknowledgments.** This work was supported by NASA.
[17] The Editor thanks two anonymous reviewers for their assistance in evaluating this paper.

References

Barr, A. C., and W. B. McKinnon (2007), Convection in Enceladus' ice shell: Conditions for initiation, *Geophys. Res. Lett.*, *34*, L09202, doi:10.1029/2006GL028799.

Bland, M. T., R. A. Beyer, and A. P. Showman (2007), Unstable extension of Enceladus' lithosphere, *Icarus*, *192*, 92–105, doi:10.1016/j.icarus.2007.06.011.

Bland, M. T., K. N. Singer, W. B. McKinnon, and P. M. Schenk (2012), Enceladus' extreme heat flux as revealed by its relaxed craters, *Geophys. Res. Lett.*, *39*, L17204, doi:10.1029/2012GL052736.

Běhounková, M., G. Tobie, G. Choblet, and O. Čadek (2010), Coupling mantle convection and tidal dissipation: Applications to Enceladus and Earth-like planets, *J. Geophys. Res.*, *115*, E09011, doi:10.1029/2009JE003564.

Běhounková, M., G. Tobie, G. Choblet, and O. Čadek (2012), Tidally-induced melting events as the origin of south-pole activity on Enceladus, *Icarus*, *219*, 655–664, doi:10.1016/j.icarus.2012.03.024.

Crow-Willard, E., and R. T. Pappalardo (2011), Global geological mapping of Enceladus, *EPSC-DPS Joint Meeting 2011*, p. 635, Nantes, France.

Ducci, M., et al. (2012), The geodesy of the main Saturnian satellites from range rate measurements of the Cassini spacecraft, *Lunar and Planetary Science Conference Abstracts, Lunar and Planetary Science Conference Abstracts*, vol. 43, abstract 2200, Houston, Tx.

Grott, M., F. Sohl, and H. Hussmann (2007), Degree-one convection and the origin of Enceladus' dichotomy, *Icarus*, *191*, 203–210, doi:10.1016/j.icarus.2007.05.001.

Han, L., G. Tobie, and A. P. Showman (2012), The impact of a weak south pole on thermal convection in Enceladus' ice shell, *Icarus*, *218*, 320–330, doi:10.1016/j.icarus.2011.12.006.

Hoppa, G. V., B. R. Tufts, R. Greenberg, and P. E. Geissler (1999), Formation of cycloidal features on Europa, *Science*, *285*, 1899–1902, doi:10.1126/science.285.5435.1899.

Howett, C. J. A., J. R. Spencer, J. Pearl, and M. Segura (2011), High heat flow from Enceladus' south polar region measured using 10–600 cm^{-1} Cassini/CIRS data, *J. Geophys. Res.*, *116*, E03003, doi:10.1029/2010JE003718.

Kargel, J. S., and S. Pozio (1996), The volcanic and tectonic history of Enceladus, *Icarus*, *119*, 385–404, doi:10.1006/icar.1996.0026.

McKinnon, W. B. (2013), The shape of Enceladus as explained by an irregular core: Implications for gravity, libration, and survival of its subsurface ocean, *J. Geophys. Res. Planets*, *118*, 1775–1788, doi:10.1002/jgre.20122.

Meyer, J., and J. Wisdom (2007), Tidal heating in Enceladus, *Icarus*, *188*, 535–539, doi:10.1016/j.icarus.2007.03.001.

Meyer, J., and J. Wisdom (2008), Tidal evolution of Mimas, Enceladus, and Dione, *Icarus*, *193*, 213–223, doi:10.1016/j.icarus.2007.09.008.

Mitri, G., and A. P. Showman (2008), A model for the temperature-dependence of tidal dissipation in convective plumes on icy satellites:

Implications for Europa and Enceladus, *Icarus*, *195*, 758–764, doi:10.1016/j.icarus.2008.01.010.

Moresi, L., and V. Solomatov (1998), Mantle convection with a brittle lithosphere: Thoughts on the global tectonic styles of the Earth and Venus, *Geophys. J. Int.*, *133*, 669–682, doi:10.1046/j.1365-246X.1998.00521.x.

Nimmo, F., J. R. Spencer, R. T. Pappalardo, and M. E. Mullen (2007), Shear heating as the origin of the plumes and heat flux on Enceladus, *Nature*, *447*, 289–291, doi:10.1038/nature05783.

Olgin, J. G., B. R. Smith-Konter, and R. T. Pappalardo (2011), Limits of Enceladus's ice shell thickness from tidally driven tiger stripe shear failure, *Geophys. Res. Lett.*, *38*, L02201, doi:10.1029/2010GL044950.

O'Neill, C., and F. Nimmo (2010), The role of episodic overturn in generating the surface geology and heat flow on Enceladus, *Nat. Geosci.*, *3*, 88–91, doi:10.1038/ngeo731.

Porco, C. C., et al. (2006), Cassini observes the active south pole of Enceladus, *Science*, *311*, 1393–1401, doi:10.1126/science.1123013.

Postberg, F., J. Schmidt, J. Hillier, S. Kempf, and R. Srama (2011), A salt-water reservoir as the source of a compositionally stratified plume on Enceladus, *Nature*, *474*, 620–622, doi:10.1038/nature10175.

Roberts, J. H., and F. Nimmo (2008), Tidal heating and the long-term stability of a subsurface ocean on Enceladus, *Icarus*, *194*, 675–689, doi:10.1016/j.icarus.2007.11.010.

Showman, A. P., and L. Han (2005), Effects of plasticity on convection in an ice shell: Implications for Europa, *Icarus*, *177*, 425–437, doi:10.1016/j.icarus.2005.02.020.

Tackley, P. J. (2000), Mantle convection and plate tectonics: Toward an integrated physical and chemical theory, *Science*, *288*, 2002–2007, doi:10.1126/science.288.5473.2002.

Tobie, G., O. Čadek, and C. Sotin (2008), Solid tidal friction above a liquid water reservoir as the origin of the south pole hotspot on Enceladus, *Icarus*, *196*, 642–652, doi:10.1016/j.icarus.2008.03.008.

Waite, J. H. Jr., et al. (2009), Liquid water on Enceladus from observations of ammonia and ^{40}Ar in the plume, *Nature*, *460*, 487–490, doi:10.1038/nature08153.

Zhong, S., M. T. Zuber, L. Moresi, and M. Gurnis (2000), Role of temperature-dependent viscosity and surface plates in spherical shell models of mantle convection, *J. Geophys. Res.*, *105*, 11,063–11,082, doi:10.1029/2000JB900003.